THE JOURNAL OF PHYSICAL CHEMISTRY C

Subscriber access provided by UNIV OF NEW ENGLAND ARMIDALE

C: Surfaces, Interfaces, Porous Materials, and Catalysis

Tuning the Hydrophobicity of Layer-Structure Silicates to Promote Adsorption of Non-Aqueous Fluids: Effects of F for OH Substitution on CO Partitioning into Smectite Interlayers

Narasimhan Loganathan, A. Ozgur Yazaydin, R. James Kirkpatrick, and Geoffrey M Bowers

J. Phys. Chem. C, **Just Accepted Manuscript** • DOI: 10.1021/acs.jpcc.8b11296 • Publication Date (Web): 11 Feb 2019

Tuning the Hydrophobicity of Layer-Structure Silicates to Promote Adsorption of Non-Aqueous Fluids: Effects of F^- for OH^- Substitution on CO_2 Partitioning into Smectite Interlayers

Narasimhan Loganathan[1], A. Ozgur Yazaydin[1,2], R. James Kirkpatrick[1,3] and Geoffrey M. Bowers[4]*

[1] Department of Chemistry, Michigan State University, East Lansing, Michigan 48824, United States

[2] Department of Chemical Engineering, University College London, London, WC1E7JE, United Kingdom

[3] Department of Earth and Environmental Sciences, Michigan State University, East Lansing, Michigan 48824, United States

[4] Department of Chemistry and Biochemistry, St. Mary's College of Maryland, St. Mary's City, Maryland 20686, United States

[*] **Corresponding author e-mail:** naresh20@msu.edu

Abstract

The intercalation of non-aqueous fluids in the nanopores of organic and inorganic materials is of significant interest, particularly in the energy science community. Recently, XRD and computational modeling results have shown that structural F^- for OH^- substitution in layered silicates makes them more hydrophobic. Here, we use Grand Canonical Molecular Dynamics (GCMD) calculations to investigate how increasing the $F^-/(F^-+OH^-)$ ratio of a prototypical layered silicate (the smectite Na-hectorite) impacts the intercalation behavior of CO_2 and H_2O at elevated temperature and pressure. At the conditions of this study (T = 323 K, P = 90 bar, water-saturated CO_2), increasing F^- for OH^- substitution causes decreasing total CO_2+H_2O intercalation, increasing $CO_2/(CO_2+H_2O)$ ratios in the interlayer galleries, and an increasing energy barrier to CO_2 and H_2O intercalation. CO_2 intercalation is greatest at monolayer basal spacings, and the results support the idea that with Na^+ as the exchangeable cation the interlayers must be propped open by some H_2O molecules to allow CO_2 to enter the interlayer galleries. The computed immersion energies suggest that the bilayer or a more expanded structure is the stable state under these conditions, in agreement with experimental results, and that the basal spacings of the minimum energy 2L structures increase with increasing F^- for OH^- substitution. These results are consistent with a wide range of experimental data for smectites at ambient conditions and elevated pressures and temperatures and suggest that F^- for OH^- substitution in conjunction with reduced structural charge and exchange with large, low charge cations may increase the ability of smectite minerals to incorporate hydrophobic species such as CH_4, CO_2, H_2, and other organic compounds.

Introduction

Oxide materials have a wide range of hydrophobicities that depend on the complex interactions among their structure, permanent and pH-dependent charge, and functionalization of their surface sites.[1-3] Among the layer structure silicates (phyllosilicates), phases with no permanent structural charge such as talc and pyrophyllite are more hydrophobic than those with a permanent charge, such as micas and smectite clays.[4-6] In addition, heterogenous charge distribution created by isomorphic cation substitution can result in local variations in hydrophobicity, which can affect the adsorption of water molecules, ions and organic species.[7-9] For instance, experimental studies by Rana et al.[7] suggest that the greater affinity of dibenzo-*p*-dioxin for Cs-saponite than Cs-montmorillonite is related to such local structural effects. Saponite has Al^{+3} for Si^{+4} substitution in the tetrahedral sheet, whereas montmorillonite has only Mg^{+2} for Al^{+3} substitution in the octahedral sheet. They propose that the strong adsorption of Cs^{+} ions at the centers of ditrigonal cavities near the Al[4] sites (a favorable cation adsorption site as suggested by molecular modeling[9]) makes the interlayer space between cations readily available to charge-neutral organic species, presumably by impacting the local hydrophobicity. Furthermore, their studies show that the cation hydration energy plays a critical role in determining the adsorption of organic species, with large ions with low hydration energies allowing greater uptake of organics (e.g., $Cs^{+} > Rb^{+} > K^{+} > Na^{+}$). Smectites have been shown to adsorb many different kinds of charged and charge neutral organic and inorganic species in their interlayers and on their external surfaces.[7,8,10,11] Together, these studies suggest that a range of local hydrophobicities is possible in layered silicates and that the hydrophobicity is influenced by the H_2O affinity of the cation.

Structural properties can also influence the hydrophobicity of porous materials. For example, it is well known that F^{-} for OH^{-} substitution increases the hydrophobicity of metal organic

frameworks and 3D porous silicates such as zeolites.[12-15] However, less is known about the effects of F^- for OH^- substitution on smectite clays and their interactions with aqueous and non-aqueous fluids. XRD studies by Dazas et al.[16,17] show that F^- for OH^- substitution in smectites reduces the interlayer H_2O content by 30%. Computational molecular dynamics (MD) modeling studies by Rotenberg et al.[4] have suggested that the hydrophobicity of talc increases with F^- for OH^- substitution but that the hydrophobicity also depends strongly on the competition between the adhesion and cohesive forces of H_2O that vary with relative humidity (R.H.). Importantly, a recent FTIR and computational study by Schnetzer et al.[18] has shown that the orientation of the OH^- group in the octahedral sheet influences the interlayer H_2O content and its binding energy with the basal surfaces of smectites. A systematic study of smectite interactions with non-aqueous fluids as a function of the $F^-/(F^-+OH^-)$ ratio has yet to be performed.

Here we report the results of Grand Canonical Molecular Dynamics (GCMD) calculations exploring the effects of F^- for OH^- substitution on the incorporation of CO_2 and H_2O in the interlayer galleries of the prototypical smectite mineral, hectorite. It is now well known that CO_2 can intercalate the interlayer galleries of smectite clays under certain circumstances,[19-41] particularly when the interlayer is propped open by a small amount of interlayer adsorbed H_2O[19-38] or when the interlayer contains large cations with comparable solvation energies for CO_2 and H_2O (e.g. Cs^+).[39-41] The calculations presented here show that at a given basal spacing (interlayer thickness) increasing F^- for OH^- substitution causes a progressive decrease in the amount of intercalated H_2O and an increase in the $CO_2/(CO_2+H_2O)$ ratio. The structural sites occupied by F^- and OH^- in the tetrahedral-octahedral-tetrahedral (T-O-T) structure of 2:1 layer silicates are part of the central, octahedral sheet and are therefore not part of the basal surface oxygen (O_b) layer with which the interlayer species interact most directly (Figure 1). For this reason, F^- for OH^-

substitution is often thought to have relatively modest effects on the interlayer fluid behavior. The results here, however, show that for smectites in contact with supercritical, H_2O-saturated CO_2 the effects are substantial.

Methods

The methods employed here are similar to those used in our recent GCMD studies of the intercalation of dry and H_2O-saturated CO_2 in hectorite with no F^- for OH^- substitution,[38-41] except that the OH^- sites have from 0 to 100% F^- substitution. The simulated base hectorite model has a structural formula of $Na_{0.8}(Mg_{5.2}Li_{0.8})Si_8O_{20}(OH,F)_4$.[42] Six different models were constructed with this composition but with structural $F^-/(F^- + OH^-)$ contents of 0%, 25%, 53%, 75%, 87% and 100%. The model with 53% F^- substitution has a composition similar to the natural San Bernardino hectorite (Clay Mineral Society SHCa-1) used in many spectroscopic studies by our group and others, which has 55% F^- substitution.[21,42,43] Individual F^- ions occur in two different structural environments in the simulation models: (i) coordinated to 3 Mg octahedra and (ii) coordinated to 2 Mg and 1 Li octahedra. The ratio of these two sites used in the simulations is 60:40 in accordance with experimental ^{19}F NMR results for the natural San Bernardino sample.[43] The force field parameters for F^- are those of Marry et al.,[44] which assign identical charges on F^- and OH^-. As in our earlier studies of H_2O-saturated supercritical CO_2,[38] the OH^- groups were kept flexible (free to probe perpendicular and non-perpendicular orientations) because of their influence on the interlayer fluid content, as reported by Schentzer et al.[18] The simulations were performed at 50°C and 90 bar fluid pressure, with the external supercritical CO_2 fluid saturated in H_2O, leading to a $CO_2/(CO_2+H_2O)$ ratio of 99.6% in the fluid reservoir. Details of the simulation methods and analysis are discussed in greater detail in our previous papers and in the Supplementary Material of this paper.[38-41,45,46] For the remainder of this discussion, we define the 1L spacing for each clay

composition as the one with the maximum CO_2 content (near 12.2 Å), and the 2L spacing as the stable state determined from the immersion energies, as discussed below.

Results

The computational results show that at basal spacings equal to or greater than a 1L structure (>~12.5 Å), increasing F^- for OH^- substitution reduces the total number of interlayer-adsorbed fluid molecules (H_2O+CO_2) at all basal spacings (Figure 2). Overall, the computational results show that the total number of intercalated fluid molecules increases with increasing basal spacing, as expected. The total number of intercalated fluid molecules at basal spacings < ~12.0 Å (Figure 2 inset) is similar for all extents of fluorination, consistent with the idea that clay-cation interactions dominate the interlayer structure at small layer separations, as reported in our previous MD studies with dry CO_2.[40] Between ~15.0 Å and 18.0 Å the number of interlayer fluid molecules increases linearly with basal spacing. The increases in this region have similar slopes, with fewer interlayer fluid molecules present in the higher $F^-/(F^-+OH^-)$ ratio models at all basal spacings. Between basal spacings of ~12.0 Å and 15.0 Å, however, the 100% OH^- model experiences a steady linear increase in the number of interlayer fluid molecules whereas the models with F^- for OH^- substitution remain at a relatively consistent number of interlayer fluid molecules for some fraction of that basal spacing window. The width of this plateau is proportional to the $F^-/(F^-+OH^-)$ ratio of the clay, with larger $F^-/(F^-+OH^-)$ ratios leading to nearly constant numbers of interlayer fluid molecules over a larger range of basal spacings. In other words, increasingly fluorinated hectorites are increasingly more resistant to intercalation of additional fluid molecules between ~12.0 Å and 15.0 Å basal spacing. This behavior is consistent with the experimental observation of increasing hydrophobicity of smectites with increasing F^- content.[16,17]

The computed intercalation behaviors of CO_2 and H_2O individually vary greatly with the $F^-/(F^-+OH^-)$ ratio, with the $CO_2/(CO_2 + H_2O)$ ratio increasing with increasing F^- substitution at all basal spacings > ~11.5 Å (Figures 3 and 4). For all systems, neither H_2O nor CO_2 intercalate at basal spacings less than ~10.2 Å. H_2O adsorption starts at ~10.3 Å, and the basal spacing at which CO_2 intercalation begins decreases from 11.2 Å to 11.0 Å with increasing $F^-/(F^-+OH^-)$ ratio. All the models exhibit a local maximum in the fraction of interlayer CO_2 molecules at the 1L spacing (~12.5 Å), with a second local maximum at basal spacings between 15.5 Å and 16.0 Å in the systems with $F^-/(F^-+OH^-)$ ratios > 0.5. All models experience a decrease in the number of intercalated CO_2 molecules at basal spacings greater than ~16 Å. However, the number of intercalated CO_2 molecules at the 1L maximum increases with increasing $F^-/(F^-+OH^-)$ ratio, and this increase is even more dramatic at the 2L maximum. At all basal spacings greater than 11.0-11.2 Å, the number of intercalated CO_2 molecules is larger at larger $F^-/(F^-+OH^-)$ ratios. The amount of intercalated H_2O increases with increasing basal spacing for all compositions, and at the spacings where CO_2 begins to intercalate (>~11.0 to 11.2Å) the amount of intercalated H_2O at a given basal spacing decreases with increasing $F^-/(F^-+OH^-)$ ratio (Figures 3 and 4), again consistent with a more hydrophobic interlayer with increasing $F^-/(F^-+OH^-)$ ratio. We also note that the rate of increase in the $CO_2/(CO_2+H_2O)$ ratio increases with increasing $F^-/(F^-+OH^-)$ ratio, indicating that even small amounts of OH^- substitution in a F-rich composition can have a substantial effect on CO_2 intercalation.

The computed immersion energies for all the simulated Na-hectorite models decrease with increasing basal spacing and reach nearly constant values at basal spacings corresponding to 2L structures (Figure 5). The slope of this relationship decreases and the basal spacing at which the immersion energies become nearly constant increases with increasing $F^-/(F^-+OH^-)$ ratio. As a

result, the basal spacings of the thermodynamically stable 2L states in equilibrium with H_2O-saturated *sc*CO_2 at T=323K and P_{fluid}=90 bars are significantly different at different $F^-/(F^-+OH^-)$ ratios. The 100% OH^- model has a minimum energy at 15.6 Å, those with 28% and 53% F^- have minima at 15.8 Å, those with 75% and 87% F^- substitution have minima at 16.6 Å, and the one with 100% F^- has a minimum at 17.0 Å. Importantly, these 2L basal spacings correspond to the interlayer separation where the number of intercalated CO_2 molecules reaches a plateau at a given $F^-/(F^-+OH^-)$ ratio (see Figure 3). The 0.6 Å difference in the basal spacing of the minimum energy 2L structures of Na-hectorite in comparison to our previous studies is most likely due to the difference in the layer structural charge (-0.8 |e| here *vs* -1.0 |e| in the earlier work), which affects the number of interlayer cations and therefore the interlayer H_2O content.

The shallow energy minima observed for the 1L states (brown circle in Figure 5) suggests that the 2L structures are more likely to be the stable state for Na-hectorite in equilibrium with water saturated CO_2 under the pressure and temperature conditions of these simulations. This conclusion is in good agreement with previously published *in situ* high *T* and *P* experimental studies and other computational modeling studies of hectorite and the similar smectite mineral, montmorillonite.[21,22,25-30,32,33,36-38] The absence of well-defined energy minima in the 1L basal spacing range, however, contrasts with the results for Na-hectorite at ambient conditions with only H_2O,[47] likely a result of the co-intercalation of CO_2 and its influence on the interlayer energetics.

The computed immersion energies (Figure 5) also show that at low basal spacings there is a significant energy barrier to both H_2O and CO_2 intercalation at larger $F^-/(F^-+OH^-)$ ratios but that there is essentially no barrier at low $F^-/(F^-+OH^-)$ ratios at these thermodynamic conditions. Since Na-hectorite requires that the basal spacing reach ~11.2 Å due to H_2O intercalation before CO_2 can enter the interlayer, this difference at low basal spacing clearly indicates increasing

hydrophobicity with increasing F^- content. The results indicate that at large F^- contents the basal spacing should be at least 10.4 Å to overcome this energy barrier and to have a favorable interaction with the H_2O molecules. Although our results are for hectorite in contact with H_2O-saturated *sc*CO_2 at elevated T and P, this behavior is qualitatively comparable to experimentally observed H_2O adsorption data for OH- and F-hectorite at room T and P.[16] These results show that OH-hectorite readily adsorbs H_2O at low R.H.s, but that such adsorption starts only at ~10% R.H. for F^- hectorite.

For the 1L state, the atomic density profiles (ADPs) of intercalated Na^+, CO_2 and H_2O as functions of distance normal to the basal surfaces vary significantly with $F^-/(F^-+OH^-)$ ratio (Figures 6a-6f). Irrespective of the $F^-/(F^-+OH^-)$ ratio, the ADPs of C_{CO2} and O_{CO2} in the 1L state are characterized by a single peak located in the midplane of the interlayer at distances ~2.9 Å from the basal surfaces [defined here as the mean position of the basal oxygen atoms (O_b)]. As shown in our earlier study,[38] these distributions indicate that the CO_2 molecules are on average oriented with their molecular (O-C-O) axes parallel to the two basal surfaces and that their angle with respect to the basal surface experiences oscillation about this mean orientation. Because the interlayer $CO_2/(CO_2+H_2O)$ ratios increase with increasing $F^-/(F^-+OH)$ ratio in the 1L region, the ADP peak intensities of C_{CO2} and O_{CO2} increase and those of O_{H2O} and H_{H2O} decrease with increasing $F^-/(F^-+OH)$ ratio. The ADPs of O_{H2O} in the 1L structures are characterized by single peaks located at the midplane of the interlayer region sharing the same plane as that of the CO_2 molecules, along with shoulders closer to the two basal surfaces. These shoulders become more prominent with increasing F^- content. In parallel, the ADPs of H_{H2O} vary greatly with $F^-/(F^-+OH^-)$ ratio. At 100% OH^-, the H_{H2O} ADPs are well resolved with two peaks centered at 1.8 Å from each basal surface. Based on the results from our previous simulation study of Na-hectorite with 100%

OH^- under the identical thermodynamic conditions,[38] these H_2O molecules are oriented with 1 H_{H2O} atom pointed towards the basal surface and the other involved in H-bonding with other H_2O molecules. At 28% and 53% F^-, the H_{H2O} ADPs become flatter, with four less well resolved peaks at 1.8 Å and 2.6 Å from each basal surface. This change is due to an increasing number of H_2O molecules that are not participating in a well-organized H-bonding network, resulting the H_{H2O} atoms at 2.6 Å lying more parallel to the basal surfaces than at lower F^- contents. At higher F^- contents, the H_{H2O} ADPs are broader and even less well resolved due to an even larger fraction of H_2O molecules not involved in an H-bonding network, including to the O_b atoms. The computed number of H-bonds/H_2O molecule at the midplane decreases from 2.3 to 1.9 as the structural F^- content increases from 0% to 100%, supporting this conclusion. (Here we define an H-bond to occur if the O···H distance is ≤ 2.45 Å and the angle between the O···O and O-H vectors is ≤ 30º). At 100% OH^-, the ADPs of Na^+ for the 1L structures show two peaks centered ~2.5 Å from each basal surface. As described in our previous study,[38] these peaks represent Na^+ ions in inner sphere (IS) coordination above O_b atoms such that the Na^+ ions hop between the two surfaces. With increasing F^- content, the Na^+ distribution becomes broader and centered more at the midplane of the interlayer, with the resolution of the two peaks decreasing. These changes are probably due to the increasing association of CO_2 with the basal surfaces limiting the possibility of Na^+ coming close to them.

The ADPs of the intercalated species in the 2L structures are very different than those in the 1L structures and also vary significantly with $F^-/(F^-+OH^-)$ ratio (Figure 7a-7f). At all $F^-/(F^-+OH^-)$ ratios, the C_{CO2} atoms are located in two layers located ~2.9 Å from each basal surface. In contrast, the ADPs of O_{CO2} are characterized by well-defined peaks at ~3.0 Å from each basal surface with shoulders at ~2.2 Å. These distributions indicate that on average the CO_2 molecules

lie with their O-C-O axes nearly parallel to the basal surfaces and that the angle of these axes with respect to the basal surface oscillate (see Figure S1), as in the 1L case and our previous studies of CO_2 in Na-smectite.[33,38] These results show that even with H_2O present the CO_2 molecules are less dynamically restricted and probe more O-C-O orientations in the 2L state than in the 1L state. The C_{CO2} and O_{CO2} ADPs are nearly unobservable at low F^- contents due to the low number of intercalated CO_2 molecules at these conditions, and their intensities increase with increasing $F^-/(F^- + OH^-)$ ratio as the mole fraction of CO_2 increases. As a result, although the mean orientation of the O-C-O vector is parallel to the basal surfaces for all models, the intensities of the ADPs are very small in the 100% OH- hectorite models in comparison to those with high F^--contents (Figure S1).The ADPs of H_2O molecules in the 2L structures are more influenced by the presence of the structural F^- atoms (Figures 7a-7f), as expected if the hydrophobicity of the surface increases with increasing F^-. For the 100% OH^- model, the O_{H2O} ADP contains four peaks at 2.8 Å and 4.1 Å from each basal surface. In parallel, the H_{H2O} ADP for this composition contains four peaks at 1.8 Å and 3.1 Å from each basal surface. The approximately equal intensities of the peak for O_{H2O} at 2.8 Å and the H_{H2O} peak at 1.8 Å suggest that the adsorption environment of these H_2O molecules is similar to that in the 1L state, with one-atom pointing towards the basal surface and the other forming H-bonds with other H_2O molecules. At 28% and 53% F^-, these distributions are similar to those at 100% OH^-, except that the relative intensities of the O_{H2O} and H_{H2O} closest to the basal surfaces decrease, indicating that the fraction of H_2O molecules coordinating the basal surfaces decreases with increasing F^- content. At higher F^- contents, the O_{H2O} and H_{H2O} ADPs are different (Figures 7a-7c). The ADPs of O_{H2O} show a peak at 2.9 Å from each basal surface and a single peak at the midplane of the interlayer. In parallel, the ADPs of H_{H2O} contain six peaks centered at 2.0 Å, 3.0 Å and 4.5 Å from each basal surface. The H_2O molecules with their O_{H2O} near 3.0Å are in

adsorption environments similar to those in the 1L state and at higher OH^- contents in the 2L state. Those at 5.0 Å are engaged in H-bonding among themselves and with the molecules at 3.0 Å, but not with the O_b atoms. The relative intensities of the various O_{H2O} and H_{H2O} ADP peaks vary little for the 75%, 87%, and 100% F^- compositions.

The increasing interlayer CO_2 content with increasing $F^-/(F^-+OH^-)$ ratios has a significant effect on the adsorption environments of Na^+ in the 2L structures. At 0%, 28%, and 53% F^-, the majority of the Na^+ ions are adsorbed in outer sphere (OS) surface complexes, as shown by the ADP peak at the midplane of the interlayer. A small fraction is adsorbed in IS coordination (ADP peak centered at 2.7Å from each basal surface), as in the 1L state. This distribution is very similar to those in our previous modeling studies of Na-hectorite with 100% OH^- at 323K and 90 bars and at ambient conditions.[21,38] In contrast, at higher F^- contents (Figures 7a-7c) the Na^+ ADPs show a peak at 2.9 Å from each basal surface and a flat distribution in the middle of the interlayer region. The increased intensity at 2.9 Å demonstrates that a greater fraction of the Na^+ ions occur in IS coordination to the basal surface, and the broad distribution indicates that they are moving through the middle of the interlayer region as they exchange from one basal surface to the other. Thus, the decreasing association of H_2O molecules with the basal surfaces and the larger interlayer CO_2 mole fractions caused by the increasing hydrophobicity of the clay due to the increasing $F^-/(F^-+OH^-)$ ratio results in different Na^+ environments than in the single crystal XRD studies of Kalo et al.,[48] which show only outer sphere Na^+ in fluorohectorites with only H_2O at low T (173 K). Further details about the coordination environments of Na^+ in our different hectorite models are discussed in the Supporting Information (Figure S2).

Discussion and Implications

The computed changes in the intercalation behavior of CO_2 and H_2O in Na-hectorite with varying $F^-/(F^-+OH^-)$ ratio clearly demonstrate that F^- for OH^- substitution on the smectite octahedral sheet increases smectite hydrophobicity. The overall influence on the H_2O uptake behavior parallels that of F^- for OH^- substitution on the surfaces of silicas and in zeolites and fluorinated metal organic frameworks,[1-3, 12-15] even though the F-sites are not directly on the external surfaces. The substantial changes in the intercalation properties of Na-hectorite with increasing $F^-/(F^-+OH^-)$ ratio is correlated to two key features of the calculations: (i) the location and Lennard-Jones parameters of the F^- ions and (ii) the orientations of OH^- groups. The F^- have the same charge as OH^- and are structural located beneath the centers of the ditrigonal cavities. The size and regularity of these cavities allow the F^- to influence the composition and structural environments of the fluid species and exchangeable cations in the interlayer galleries and on external particle surfaces. The effects of the orientation of the OH^- groups is due to the majority of them being oriented with their O-H vectors perpendicular to the basal surfaces. This orientation significantly alters the local charge distribution relative to sites occupied by F^-, because of the presence of positive charge near tetrahedral layer. Moreover, our previous simulation studies of Na-hectorite with 100% OH^- have also shown that the orientation of the structural OH^- groups impacts the interlayer fluid content, structure and dynamics under similar thermodynamic conditions.[38] These conclusions are in good agreement with the experimental IR and H_2O sorption study of Schnetzer et al.,[18] which shows that OH^- in hectorite is responsible for increased affinity towards H_2O based on changes in the frequency of the δ(Al-OH-Mg) band. The 30% decrease in interlayer H_2O content at ambient conditions due to F^- for OH^- substitution reported by Dazas et al.[16] is very similar to the differences at 2L basal spacings for complete F^- and OH^- substitution in our simulations. The progressively larger energy barrier to H_2O intercalation into collapsed

hectorite interlayers with increasing $F^-/(F^-+OH^-)$ ratio found here is also in good agreement with the different slopes of the H_2O sorption isotherms for OH^- and F^- hectorites observed by Dazas et al.[16] The increase in equilibrium basal spacing in the 2L region with increasing $F^-/(F^-+OH^-)$ ratio is probably driven by a need to increase the total number of interlayer H_2O molecules to develop a stable, more integrated H-bonding network. This result is in qualitative agreement with powder XRD data for fluorohectorite that show interlayer expansion from 1L to 2L only at relatively high R.H. (~70%) conditions.[16]

The MD results show that CO_2 is preferentially associated with the basal surface regardless of the presence of fluorine, resulting in a larger fraction of the H_2O molecules being located in the midplane at 2L basal spacings. This association, combined with the decreasing interlayer H_2O content in the fluorinated samples, also leads to an increasing fraction of Na^+ ions in IS coordination by the O_b atoms with increasing fluorination. These changes are probably driven by a combination of two factors: (i) disruption of the H-bonding network among H_2O molecules due to the presence of CO_2 and (ii) positive non-bonded interactions among CO_2 molecules resulting in their clustering.[39-42,49]

The intercalation behavior of smectite interlayers depends upon many factors, including total structural charge, charge location, the properties of charge compensating cations, orientation of structural OH^- groups, the composition and properties of the external fluid phase, and as this study shows, the $F^-/(F^-+OH^-)$ ratio of the octahedral sheet. The increasing $CO_2/(CO_2+H_2O)$ ratio with $F^-/(F^-+OH^-)$ ratio suggests that F^- for OH^- substitution should result in increased capacity to sorb non-polar species such as CH_4 and other small hydrocarbons.[43] Exchangeable cations with similar solvation energies for H_2O and CO_2[50] are also known to increase CO_2 intercalation,[40,41] and should work in parallel with F^- for OH^- substitution to increase this capacity even more. The

number of divalent cations needed for charge balance is half that of monovalent cations, resulting in more free volume in the interlayer. Exchange of such cations, especially larger ones such as Sr^{2+} and Ba^{2+}, in combination with F^- for OH^- substitution are also likely to increase smectite sorption capacity for hydrophobic species. Computational studies have shown that reducing the structural charge on the clay enhances CO_2 intercalation,[37] and this may also contribute to intercalation of other hydrophobic species. As illustrated by recent experimental studies, the composition of the external fluid phase strongly affects the intercalation, with high H_2O activities suppressing CO_2 intercalation[21,28-31,43] and presumably that of other hydrophobic species. It also seems likely that even with F^- substitution, small linear and planar molecules should be more easily incorporated than large ones with complex molecular structures.

The results here suggest that F^- for OH^- substitution can be used as a tool to regulate the local hydrophobic and hydrophilic properties of phyllosilicates and other aluminosilicate materials, thereby increasing their interaction with CO_2, hydrocarbons, and other non-polar species. For instance, increased clay hydrophobicity could substantially enhance its sorption properties in waste water treatment, hydrocarbon removal in industrial processes, and in oil spill sites. In addition, we propose that fluorinated clay mineral substrates are potential sorbents for the removal of organic pollutants such as dioxins based on the mutual hydrophobic interactions between them and the clay.[17,18] Our studies highlight the importance of the compositional and structural properties of aluminosilicates in determining the wetting behavior (contact angle) of polar fluids in coating applications. Fluorination may also assist in developing aluminosilicate minerals with superhydrophobic properties for use in catalysis and separation applications where microporosity, high surface area, and hydrophobicity are essential. Our results support, for instance, the use of such materials as fluorinated silica nanoparticles, which have recently been

reported to help reducing condensate blockage near oil wells by altering the wettability of the reservoir rocks.[51]

Conclusions

Computational molecular modeling of the intercalation behavior of CO_2 and H_2O in the interlayer galleries of Na-hectorite demonstrate progressively increasing hydrophobicity with increasing $F^-/(F^-+OH^-)$ ratio in the octahedral sheet. This behavior parallels that of fluorination of silica surfaces, zeolites and metal organic frameworks,[1-3, 12-15] even though the anion sites are not on the basal surfaces of the clays. At the conditions of this study, increasing F^- for OH^- substitution causes decreasing total CO_2+H_2O intercalation, increasing $CO_2/(CO_2+H_2O)$ ratios, and an increasing energy barrier to H_2O intercalation. CO_2 intercalation is greater at monolayer basal spacings, and as previously shown,[37,39] with Na^+ as the exchangeable cation the interlayers must be propped open by some H_2O molecules to allow CO_2 intercalation.[20,21,24-37] The computed immersion energies suggest that the bilayer or a more expanded structure is the stable state under our conditions, in agreement with experimental results,[20,25-30] and that the basal spacings of the minimum energy 2L structures increase with increasing F^- for OH^- substitution. These results are consistent with a wide range of experimental data for smectites at ambient conditions and elevated pressures and temperature.[15,16,20,21,24,25,27-30,37,47]

We note that the results here suggest that the assumption of identical charges for OH^- groups and F^- atoms in the force fields used[44] is reasonable based on the overall, qualitative agreement with experimental results. However, given the potential importance of fluorinated clays and other aluminosilicate materials to a broad range of applications, it is essential to develop more refined interaction parameters for structural F^- atoms, including ones applicable to broken edge sites.

Acknowledgements

All the calculations in this work were performed using computational resources at the National Energy Research Scientific Computing Center, which is supported by the Office of Science of the U.S. Department of Energy under ECARP No. m1649. The authors acknowledge iCER computational facility at Michigan State University for additional computational resources. The work in this manuscript was supported by the United States Department of Energy, Office of Science, Office of Basic Energy Science, Chemical science, Biosciences, and Geosciences division through the grant DE-FG02-08ER15929 (Kirkpatrick, P.I.). We also acknowledge support from the Michigan State University Foundation.

Notes

The authors declare no competing financial interest.

Supporting Information

A brief discussion of simulation methods used in this study, orientations of CO_2 molecules with respect to surface normal of Na-hectorites with varying $F^-/(F^-+OH^-)$ ratio for the 2L structures. Details of the Na^+ ions radial distribution functions and running coordination with H_2O and CO_2 for the 1L and 2L structures of Na-hectorites with varying $F^-/(F^-+OH^-)$ ratio.

References

1. Coffinier, Y.; Janel, S.; Addad, A.; Blossey, R.; Gengembre, L. Payen, E.; Boukherroub, R. Preparation of Superhydrophobic Silicon Oxide Nanowire Surfaces. *Langmuir* **2007,** *23*, 1608-1611.
2. Shi, S.; Wang, M.; Chen, C.; Lu, F.; Zheng, H.; Xu, J. Preparation of Hydrophobic Hollow Silica Nanospheres with Porous Shells and their Application in Pollutant Removal. *RSC Adv.* **2013,** *3*, 1158-1164.
3. Yang, D.; Xu, Y.; Wu, D.; Sun, Y.; Zhu, H.; Deng, F., Super Hydrophobic Mesoporous Silica with Anchored Methyl Groups on the surface by a One-Step Synthesis without Surfactant Template. *J. Phys. Chem. C* **2007,** *111*, 999-1004.
4. Rotenberg, B.; Patel, A. J.; Chandler, D. Molecular Explanation for Why Talc Surfaces can be Both Hydrophilic and Hydrophobic. *J. Am. Chem. Soc.* **2011,** *133*, 20521-20527.
5. Wang, J.; Kalinichev, A. G.; Kirkpatrick, R. J. Effects of Substrate Structure and Composition on the Structure, Dynamics and Energetics of Water at Mineral Surfaces: A Molecular Dynamics Modeling Study. *Geochim. Cosmochim. Acta* **2006,** *70*, (3), 562-582.
6. Ou, X.; Lin, Z.; Li, J. Surface Microstructure Engenders Unusual Hydrophobicity in Phyllosilicates. *Chem. Commun.* **2018,** *54*, 5418-5421.
7. Rana, K.; Boyd, S. A.; Teppen, B. J.; Li, H.; Liu, C.; Johnston, C. T. Probing the Microscopic Hydrophobicity of Smectite Surfaces: A Vibrational Spectroscopic Study of Dibenzo-*p*-dioxin Sorption to Smectite. *Phys. Chem. Chem. Phys.* **2009,** *11*, 2976-2985.
8. Liu, C.; Li, H.; Teppen, B. J.; Johnston, C. T.; Boyd, S. A. Mechanisms Associated with the High Adsorption of Dibenzo-*p*-dioxin from Water by Smectite Clays. *Environ. Sci. Technol.* **2009,** *43*, 2777-2783.
9. Loganathan, N.; Kalinichev, A. G. Quantifying the Mechanisms of Site-Specific Ion Exchange at an Inhomogeneously Charged Surface. Case of Cs^+/K^+ on Hydrated Muscovite Mica *J. Phys. Chem. C* **2017**, *121*, 7829-7836.
10. Jaynes, W. F.; Boyd, S. A. Hydrophobicity of Siloxane Surfaces in Smectites as Revealed by Aromatic Hydrocarbon Adsorption from Water. *Clays Clay Miner*. **1991**, *39*, 428−436.
11. Sheng, G.; Johnston, C. T.; Teppen, B. J.; Boyd, S. A. Potential Contributions of Smectite Clays and Organic Matter to Pesticide Retention in Soils. *J. Agric. Food Chem.* **2001**, *49*, 2899-2907.
12. Zhang, K.; Lively, R. P.; Noel, J. D.; Dose, M. E.; McCool, B. A.; Chance, R. R.; Koros, W. J. Adsorption of Water and Ethanol in MFI-Type Zeolites. *Langmuir* **2012,** *28*, 8664-8673.
13. Trzpit, M.; Soulard, M.; Patarin, J.; Desbiens, N.; Cailliez, F.; Boutin, A.; Demachy, I.; Fuch, A. H. The Effect of Local Defects on Water Adsorption in Silicalite-1 Zeolite: A Joint Experimental and Molecular Simulation Study. *Langmuir* **2007,** *23*, 10131-10139.
14. Kanezashi, M.; Murata, M.; Nagasawa, H.; Tsuru, T. Flourine Doping of Microporous Organosilica Membranes for Pore Size Control and Enhanced Hydrophobic Properties. *ACS Omega* **2018,** *3*, 8612-8620.

15. Yang, C.; Kaipa, U.; Mather, Q. Z.; Wang, X.; Nesterov, V.; Venero, A. F.; Omary, M. A. Fluorous Metal-Organic Frameworks with Superior Adsorption and Hydrophobic Properties Toward Oil Spill Cleanup and Hydrocarbon Storage. *J. Am. Chem. Soc* **2011,** *133*, 18094-18097.

16. Dazas, B.; Lanson, B.; Breu, J.; Robert, J.-L.; Pelletier, M.; Ferrage, E. Smectite Fluorination and its Impact on Interlayer Water Content and Structure: A Way to Fine Tune the Hydrophilicity of Clay Surfaces. *Micro. Meso. Mat.* **2013,** *181*, 233-247.

17. Dazas, B.; Lanson, B.; Delville, A.; Robert, J.-L.; Komarneni, S.; Michot, L. J.; Ferrage, E. Influence of Tetrahedral Layer Charge on the Organization of Interlayer Water and Ions in Synthetic Na-Saturated Smectites. *J. Phys. Chem. C* **2015,** *119*, 4158-4172.

18. Schnetzer, F.; Johnston, C. T.; Premachandra, G. S.; Giraudo, N.; Schuhmann, R.; Thissen, P.; Emmerich, K. Impact of Intrinsic Structural Properties on the Hydration of 2:1 Layer Silicates. *ACS Earth Space Chem.* **2017,** *1*, 608-620.

19. Busch, A.; Bertier, P.; Gensterblum, Y.; Rother, G.; Spiers, C. J.; Zhang, M.; Wentinck, H. M. On Sorption and Swelling of CO_2 in Clays. *Geomech. Geophys. Geo-energ. Geo-resour.* **2016,** *2*, 111-130.

20. Hamm, L. M.; Bourg, I. C.; Wallace, A. F.; Rotenberg, B. Molecular Simulation of CO_2- and CO_3-Brine-Mineral Systems. *Reviews in Mineralogy and Geochemistry* **2013,** *77*, 189-228.

21. Bowers, G. M.; Schaef, H. T.; Loring, J. S.; Hoyt, D. W.; Burton, S. D.; Walter, E. D.; Kirkpatrick, R. J. Role of Cations in CO_2 Adsorption, Dynamics and Hydration in Smectite Clays under In Situ Supercritical CO_2 Conditions. *J. Phys. Chem. C* **2017,** *121*, 577-592.

22. Giesting, P.; Guggenheim, S.; van Groos, A. F. K.; Busch, A. Interaction of Carbon Dioxide with Na-Exchanged Montmorillonite at Pressures to 640 bar: Implications for CO_2 Sequestration. *Int. J. Green. Gas Cont.* **2012,** 8, 73-81.

23. Bowers, G. M.; Hoyt, D. W.; Burton, S. D.; Ferguson, B. O.; Varga, R.; Kirkpatrick, R. J. In Situ ^{13}C and ^{23}Na Magic Angle Spinning NMR Investigation of Supercritical CO_2 Incorporation in Smectite-Natural Organic Matter Composites. *J. Phys. Chem. C* **2014,** *118*, 3564-3573.

24. Lee, M.-S.; McGrail, B. P.; Glezakou, V.-A. Microstructural Response of Variably Hydrated Ca-rich Montmorillonite to Supercritical CO_2. *Environ. Sci. Technol.* **2014,** 48, 8612-8619.

25. Ilton, E. S.; Schaef, H. T.; Qafoku, O.; Rosso, K. M.; Felmy, A. R. In Situ X-ray Diffraction Study of Na^+ Saturated Montmorillonite Exposed to Variably Wet Supercritical CO_2. *Environ. Sci. Technol.* **2012,** 46, 4241-4248.

26. Rother, G.; Ilton, E. S.; Wallacher, D.; Hauss, T.; Schaef, H. T.; Qafoku, O.; Rosso, K. M.; Felmy, A. R.; Krukowski, E. G.; Stack, A. G.; et al. CO_2 Sorption to Subsingle Hydration Layer Montmorillonite Clay Studies by Excess Sorption and Neutron Diffraction Measurements. *Environ. Sci. Technol.* **2013,** 47, 205-211.

27. Schaef, H. T.; Ilton, E. S.; Qafoku, O.; Martin, P. F.; Felmy, A. R.; Rosso, K. M. In Situ X-RD study of Ca^{2+} Saturated Montmorillonite (STx-1) Exposed to Anhydrous and Wet Supercritical Carbon Dioxide. *Int. J. Green. Gas Cont.* **2012,** 6, 220-229.

28. Schaef, H. T.; Loring, J. S.; Glezakou, V. A.; Miller, Q. R. S.; Chen, J.; Owen, A. T.; Lee, M.-S.; Ilton, E. S.; Felmy, A. R.; McGrail, B. P. et al. Competitive Sorption of CO_2 and H_2O in 2:1 Layer Phyllosilicates. *Geochim. Cosmochim. Acta* **2015,** 161, 248-257.

29. Loring, J. S.; Schaef, H. T.; Turcu, R. V. F.; Thompson, C. J.; Miller, Q. R.; Martin, P. F.; Hu, J.; Hoyt, D. W.; Qafoku, O.; Ilton, E. S.; et al. In Situ Molecular Spectroscopic Evidence for CO_2 Intercalation into Montmorillonite in Supercritical Carbon Dioxide. *Langmuir* **2012,** *28*, 7125-7128.

30. Loring, J.S.; Ilton, E.S.; Chen, J.; Thompson, C.J.; Martin, P.F.; Benezeth, P.; Rosso, K.M.; Felmy, A.R.; Schaef, H.T. In Situ Study of CO_2 and H_2O Partitioning Between Na-Montmorillonite and Variably Wet Supercritical Carbon Dioxide. *Langmuir* **2014,** *30*, 6120-6128.

31. Loring, J. S.; Schaef, H. T.; Thompson, C. J.; Turcu, R. V. F.; Miller, Q. R.; Chen, J.; Hu, J.; Hoyt, D. W.; Martin, P. F.; Ilton, E. S.; et al. Clay Hydration/Dehydration in Dry to Water-Saturated Supercritical CO_2: Implications for Caprock Integrity. *Energy Procedia* **2013,** *37*, 5443-5448.

32. Krukowski, E.G.; Goodman, A.; Rother, G.; Ilton, E.S.; Guthrie, G.; Bodnar, R.J. FT-IR Study of CO_2 Interaction with Na^+ Exchanged Montmorillonite. *Appl. Clay Sci.* **2015,** *114*, 61-68.

33. Botan, A.; Rotenberg, R.; Marry, V.; Turq, P.; Noetinger, B. Carbon Dioxide in Montmorillonite Clay Hydrates: Thermodynamics, Structure and Transport from Molecular Simulation. *J. Phys. Chem. C* **2010**, *114*, 14962-14969.

34. Kadoura, A.; Nair, A. K. N.; Sun, S. Molecular Simulation Study of Montmorillonite in Contact with Variably Wet Supercritical Carbon Dioxide. *J. Phys. Chem. C* **2017**, *121*, 6199-6208.

35. Myshakin, E. M.; Saidi, W. A.; Romanov, V. N.; Cygan, R. T.; Jordan, K. D. Molecular Dynamics Simulations of Carbon Dioxide Intercalation in Hydrated Na-Montmorillonite. *J. Phys. Chem. C* **2013**, *117*, 11028-11039.

36. Makaremi, M.; Jordan, K. D.; Guthrie, G. D.; Myshakin, E. M. Multiphase Monte Carlo and Molecular Dynamics Simulations of Water and CO_2 Intercalation in Montmorillonite and Beidellite. *J. Phys. Chem. C* **2015**, *119*, 15112-15124.

37. Rao, A.; Leng, Y. Effect of Layer Charge on CO_2 and H_2O Intercalations in Swelling Clays. *Langmuir* **2016**, *32*, 11366-11374.

38. Loganathan, N.; Yazaydin, A. O.; Bowers, G. M.; Kalinichev, A. G.; Kirkpatrick, R. J. Molecular Dynamics Study of CO_2 and H_2O Intercalation in Smectite Clays: Effect of Temperature and Pressure on Interlayer Structure and Dynamics in Hectorite *J. Phys. Chem. C* **2017**, *121*, 24527-24540.

39. Schaef, H. T.; Loganathan, N.; Bowers, G. M.; Kirkpatrick, R.; Yazaydin, A. O.; Burton, S. D.; Hoyt, D. W.; Ilton, E. S.; Thanthiriwatte, K. S.; Dixon, D. A. et al. Tipping Point for Expansion of Layered Aluminosilicates in Weakly Polar Solvents: Supercritical CO_2. *ACS Appl. Mater. Interf.* **2017**, *9*, 36783-36791.

40. Loganathan, N.; Bowers, G. M.; Yazaydin, A. O.; Schaef, H. T.; Loring, J.; Kalinichev, A. G.; Kirkpatrick, R. J. Clay Swelling in Dry Supercritical Carbon Dioxide: Effects of Interlayer

Cations on the Structure, Dynamics and Energetics of CO_2 Intercalation Probed by XRD, NMR and GCMD Simulations. *J. Phys. Chem. C* **2018**, *122*, 4391-4402.

41. Loganathan, N.; Bowers, G. M.; Yazaydin, A. O.; Schaef, H. T.; Loring, J.; Kalinichev, A. G.; Kirkpatrick, R. J. Competitive Adsorption of H_2O ad CO_2 in 2-Dimensional Nano-confinement: GCMD Simulations of Cs- and Ca-Hectorite *J. Phys. Chem. C* **2018**, *122*, 23460-23469.
42. Reddy, U. V.; Bowers, G. M.; Loganathan, N.; Bowden, M.; Yazaydin, A. O.; Kirkpatrick, R. J. Water Structure and Dynamics in Smectites: ^2H NMR Spectroscopy of Mg, Ca, Sr, Cs and Pb-Hectorite. *J. Phys. Chem. C* **2016,** *120*, 8863-8876.
43. Bowers, G. M.; Loring, J. S.; Schaef, H. T.; Walter, E. D.; Burton, S. D.; Hoyt, D. W.; Cunniff, S. S.; Loganathan, N.; Kirkpatrick, R. J. Interaction of Hydrocarbons with Clays under Reservoir Conditions: In Situ Infrared and Nuclear Magnetic Resonance Spectroscopy and X-ray Diffraction for Expandable Clays with Variably Wet Supercritical Methane. *ACS Earth Space Chem.* **2018,** *2*, 640-652.
44. Marry, V.; Dubois, E.; Malikova, N.; Durand-Vidal, S.; Longeville, S.; Breu, J. Water Dynamics in Hectorite Clays: Influence of Temperature Studied by Coupling Neutron Spin Echo and Molecular Dynamics. *Environ. Sci. Technol.* **2011**, *45*, 2850-2855.
45. Loganathan, N.; Yazaydin, A. O.; Bowers, G. M.; Kalinichev, A. G.; Kirkpatrick, R. J. Structure, Energetics and Dynamics of Cs^+ and H_2O in Hectorite: Molecular Dynamics Simulations with Unconstrained Substrate Surface. *J. Phys. Chem. C* **2016**, 1*20*, 10298-10310.
46. Loganathan, N.; Yazaydin, A. O.; Bowers, G. M.; Kalinichev, A. G.; Kirkpatrick, R. J. Cation and Water Structure, Dynamics and Energetics in Smectite Clays: A Molecular Dynamics Study of Ca-Hectorite *J. Phys. Chem. C* **2016**, *120*, 12429-12439.
47. Morrow, C. P.; Yazaydin, A. O.; Krishnan, M.; Bowers, G. M.; Kalinichev, A. G.; Kirkpatrick. R. J. Structure, Energetics and Dynamics of Smectite Clay Interlayer Hydration: Molecular Dynamics and Metadynamics Investigation of Na-Hectorite. *J. Phys. Chem. C* **2013**, *117*, 5172-5187.
48. Kalo, H.; Milius, W.; Breu, J. Single Crystal Structure Refinement of One- and Two-Layer Hydrates of Sodium Fluorohectorite. *RSC Adv.* **2012**, *2*, 8452-8459.
49. Sena, M. M.; Morrow, C. P.; Kirkpatrick, R. J.; Krishnan, M. Structure, Energetics, and Dynamics of Supercritical Carbon Dioxide at Smectite Mineral-Water Interfaces: Molecular Dynamics Modeling and Adaptive Force Investigation of CO_2/H_2O Mixtures Confined in Na-Montmorillonite. *Chem. Mater.* **2015**, *27*, 6946-6959.
50. Criscenti, L. J.; Cygan, R. T., Molecular Simulations of Carbon Dioxide and Water: Cation Solvation. *Environ. Sci. Technol.* **2013**, *47*, 87-94.
51. Mousavi, M. A.; Hassanajili, Sh.; Rahimpour, M. R. Synthesis of Fluorinated Nano-Silica and its Application in Wettability Alteration Near Well-Bore Region in Gas Condensate Reservoirs. *App. Surf. Sci*. **2013**, *273*, 205-214.

Figures

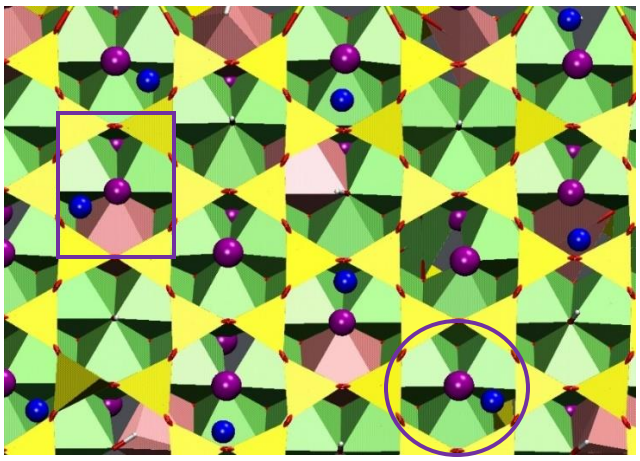

Figure 1. Schematic representation of the Na-hectorite structure with F^- atoms in 2 different octahedral environments (i) F^- coordinated to three octahedral Mg (circle). (ii) F^- coordinated to two octahedral Mg and one octahedral Li (square). Unlabeled anion sites are OH^-. Color code: yellow – Si tetrahedra; green – Mg octahedra; pink – Li octahedra; purple – F^-; blue – Na^+; Red sticks corresponds to surface oxygen atoms (O_b).

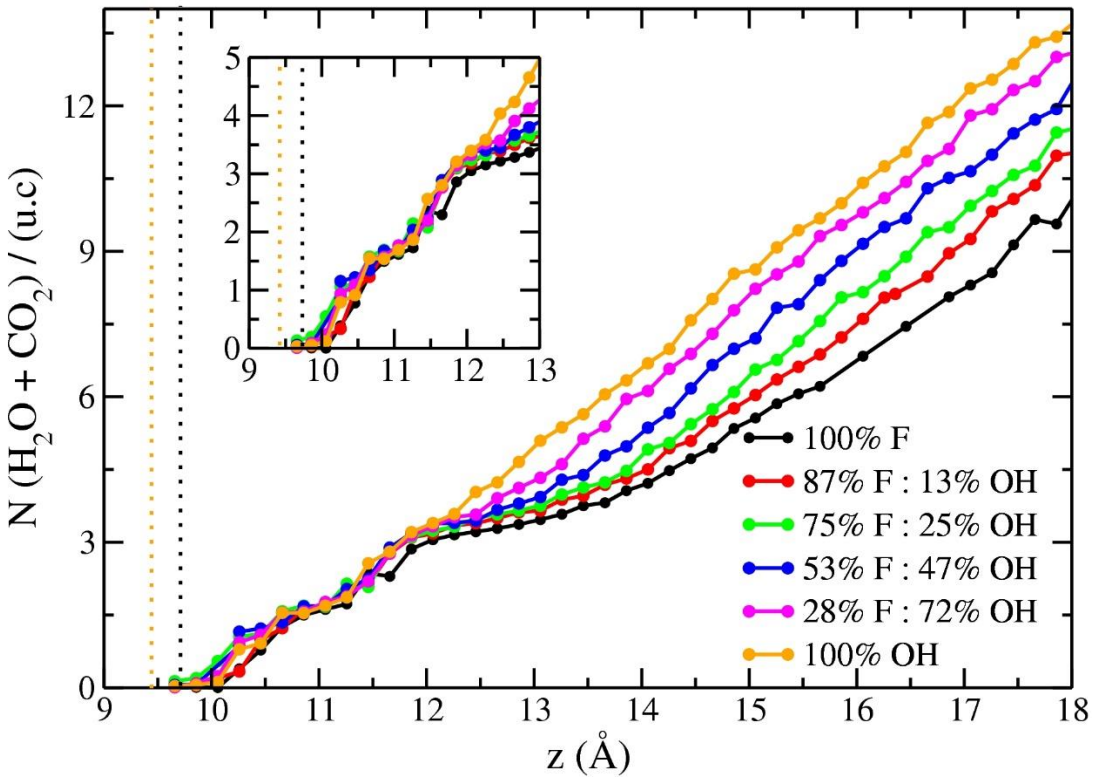

Figure 2. Computed average total number of intercalated fluid molecules (H_2O+CO_2) per unit cell in Na-hectorite with varying $F^-/(F^-+OH^-)$ ratios as functions of interlayer basal spacing at 323 K and 90 bars. Dotted vertical lines represent the collapsed basal spacing for the 100% OH^- (orange) and 100% F^- (black) hectorite models.

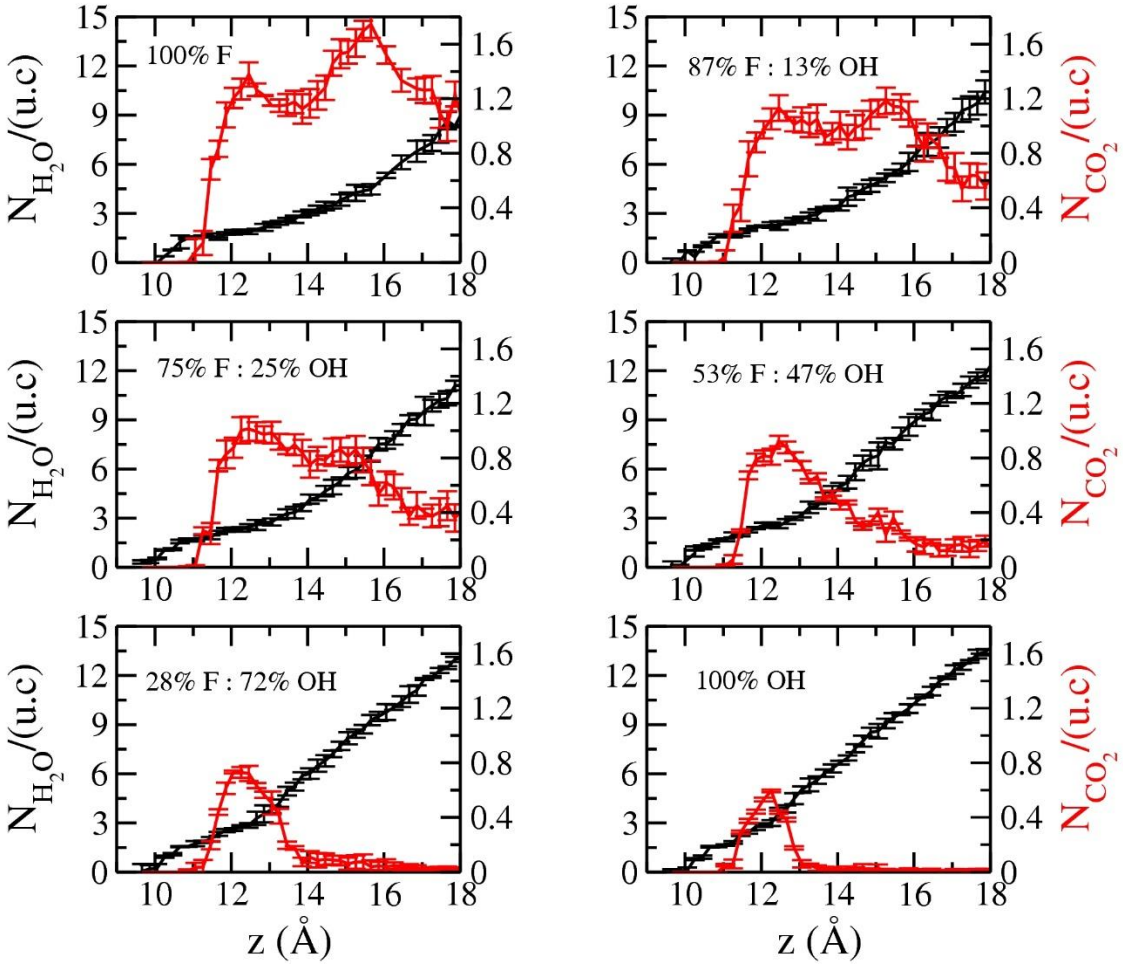

Figure 3. Computed average number of intercalated CO_2 and H_2O molecules per unit cell in Na-hectorite with varying $F^-/(F^-+OH^-)$ ratios as functions of interlayer basal spacing at 323 K and 90 bars.

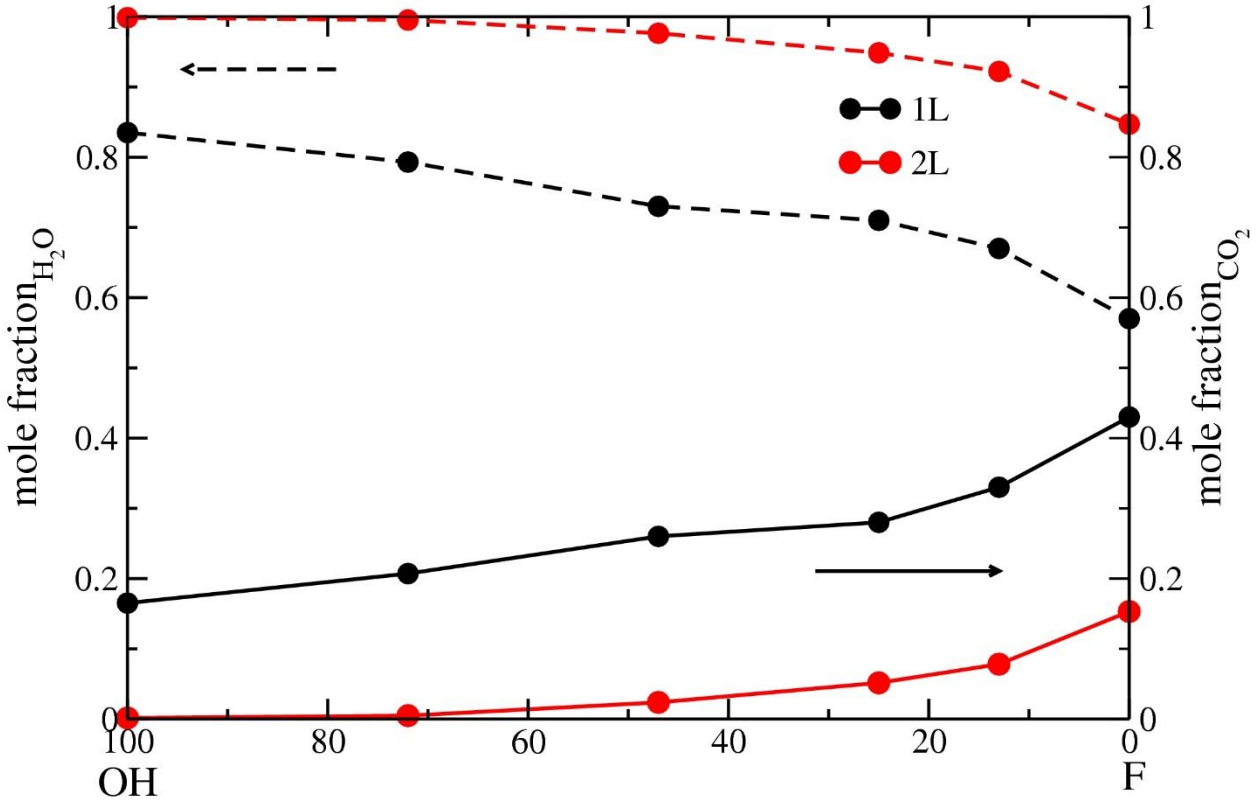

Figure 4. Computed average mole fractions of intercalated CO_2 and H_2O molecules per unit cell in Na-hectorite with varying $F^-/(F^-+OH^-)$ ratios as functions of interlayer basal spacing at 323 K and 90 bars.

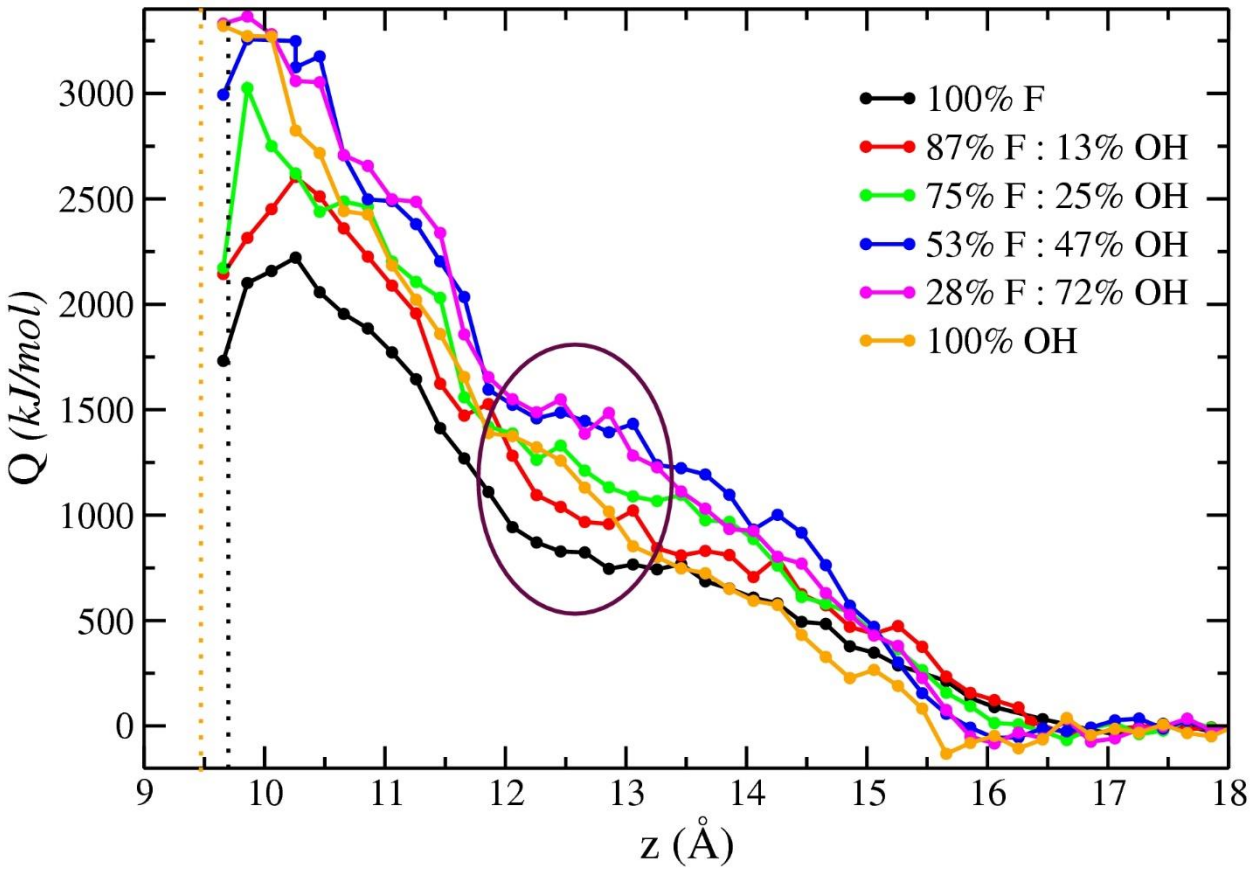

Figure 5. Computed **i**mmersion energies of Na-hectorite with intercalated CO_2 and H_2O molecules in Na-hectorite with varying $F^-/(F^-+OH^-)$ ratios as functions of interlayer basal spacing at 323 K and 90 bars. Dotted vertical lines represent the collapsed basal spacing for the 100% OH^- (orange) and 100% F^- (black) hectorite models. Brown circle indicates the shallow energy minima in different Na-hectorite models.

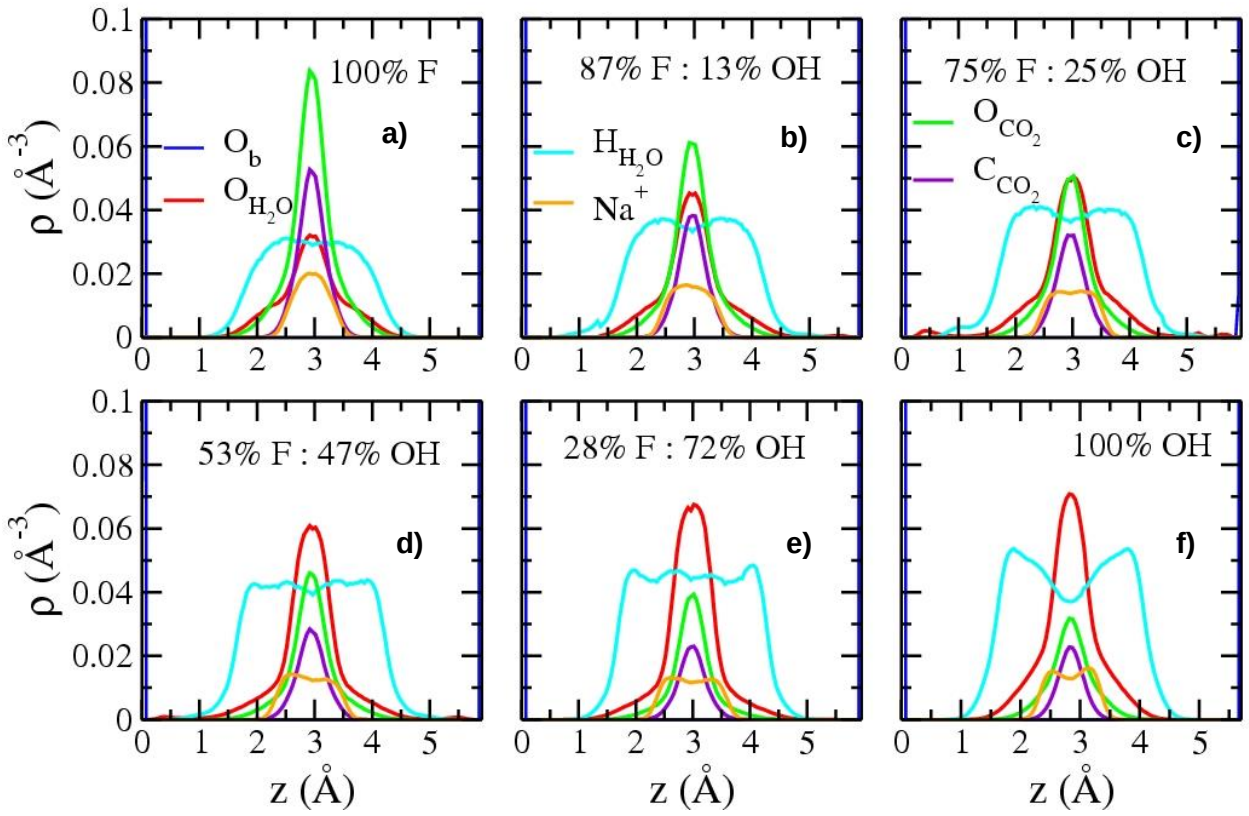

Figure 6. Computed atomic density profiles (ADPs) of Na^+ (orange), O_{CO2} (green), C_{CO2} (violet), O_{H2O} (red) and H_{H2O} (cyan) at 1L basal spacings for Na-hectorite with the indicated $F^-/(F^-+OH^-)$ ratios as functions of interlayer basal spacing at 323 K and 90 bars. The basal surfaces are defined by the average positions of the O_b atoms (dark blue vertical lines).

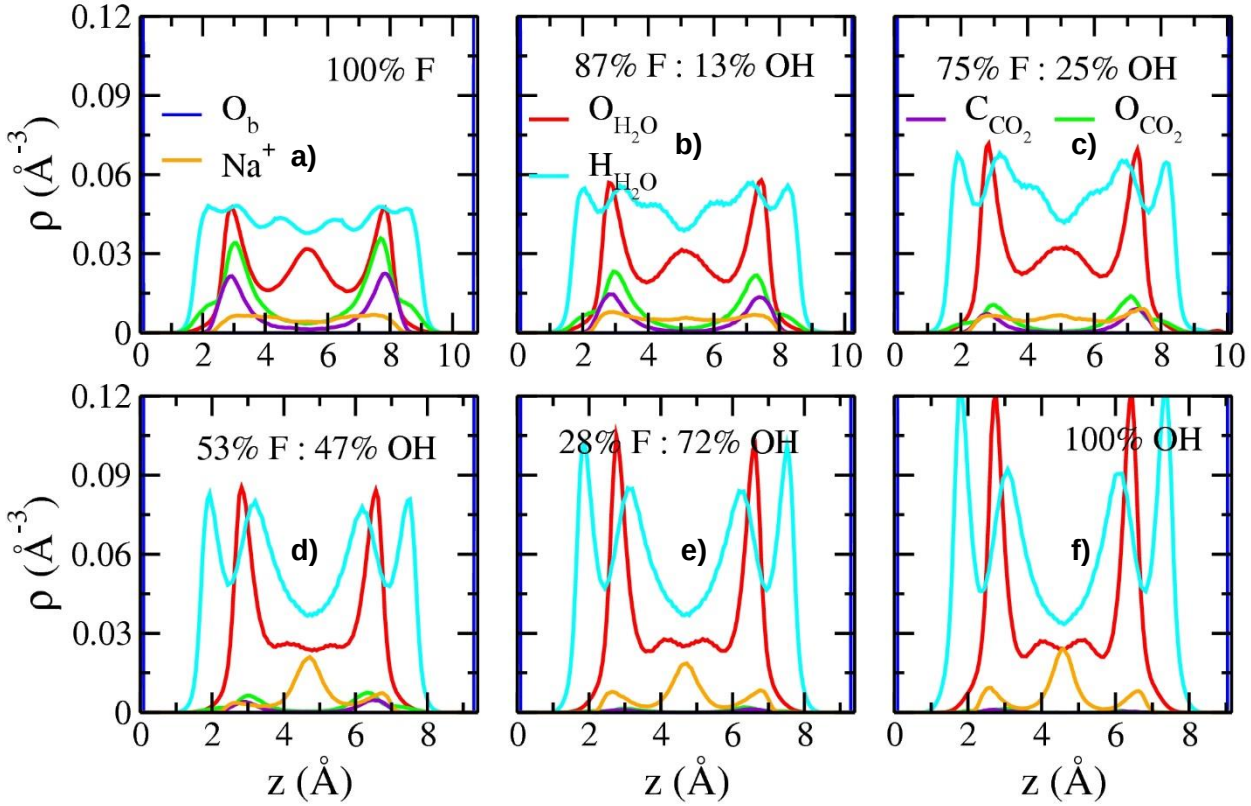

Figure 7. Computed atomic density profiles (ADPs) of Na^+ (orange), O_{CO2} (green), C_{CO2} (violet), O_{H2O} (red) and H_{H2O} (cyan) at 2L basal spacings for Na-hectorite with the indicated $F^-/(F^-+OH^-)$ ratios as functions of interlayer basal spacing at 323 K and 90 bars. The basal surfaces are defined by the average positions of the O_b atoms (dark blue vertical lines). The ADPs of O_{CO2} and C_{CO2} are enhanced two times than their actual values to improve visibility.

TOC Graphic